Chinese Journal of
POLYMER SCIENCE

RESEARCH ARTICLE

https://doi.org/10.1007/s10118-026-3822-3
Chinese J. Polym. Sci.

Radial Distribution of Crystallinity in Aramid Fibers Investigated by Raman Spectroscopy

Wei-Gen Yang[a,b], Yuan Lin[a], Hao-Jun Sun[c], and Zhao-Hui Su[a,b*]

[a] *State Key Laboratory of Polymer Science and Technology, Changchun Institute of Applied Chemistry, Chinese Academy of Sciences, Changchun 130022, China*
[b] *School of Applied Chemistry and Engineering, University of Science and Technology of China, Hefei 230026, China*
[c] *National Synchrotron Radiation Laboratory, Anhui Provincial Engineering Laboratory of Advanced Functional Polymer Film, CAS Key Laboratory of Soft Matter Chemistry, University of Science and Technology of China, Hefei 230026, China*

Electronic Supplementary Information

Abstract The skin-core morphology and the crystallinity in aramid fibers critically influence their mechanical properties. In this study, Kevlar 29 and Kevlar 49 fibers were embedded in epoxy and cut along the longitudinal direction, and the cross-sections were characterized by using confocal Raman spectroscopy. The degrees of crystallinity in the skin and the core regions were determined quantitatively, and the crystallinity profiles along the radial direction were obtained for both fibers. The results showed that the crystallinity at the fiber surface was relatively low, which increased quickly into the fiber and approached a higher plateau value at the fiber center. The Kevlar 49 exhibited a steeper increase in the skin region than Kevlar 29, and a more uniform distribution in the core region with a higher degree of crystallinity.

Keywords Poly(*p*-phenylene terephthalamide); Fibers; Skin-core structure; Raman spectroscopy; Crystallinity

Citation: Yang, W. G.; Lin, Y.; Sun, H. J.; Su, Z. H. Radial distribution of crystallinity in aramid fibers investigated by Raman spectroscopy. *Chinese J. Polym. Sci*. https://doi.org/10.1007/s10118-026-3822-3

INTRODUCTION

Poly(*p*-phenylene terephthalamide) (PPTA) fibers have attracted considerable attention owing to their outstanding mechanical properties, including high tensile strength, high modulus, and excellent impact.[1–3] Commercial aramid fibers such as Kevlar and Twaron exhibit high strength-to-weight ratios and excellent toughness. Consequently, they are widely used in ballistic armor, aerospace structures, and transportation composites[4,5] constituting critical reinforcement materials in modern defense and strategic engineering systems.[6,7]

PPTA fibers are produced by dry-jet wet spinning, which results in a highly oriented molecular structure.[8] This processing route often leads to the formation of a skin-core structure, a common heterogeneous feature of high-performance fibers.[9] The structural characteristics of the skin-core region affect the energy absorption and crack propagation during tensile deformation, thus influencing the overall mechanical behavior of the fibers.[10–12] For this reason, the skin-core structure of PPTA fibers has been investigated using different characterization methods. Dobb *et al.* studied Kevlar 49 by transmission electron microscopy (TEM) and electron diffraction and showed that there was a difference in the banded structure between the surface and the interior of the fiber.[13] Morgan and Steele characterized PPTA fibers by scanning electron microscopy (SEM) and found that the outer region of the fibers was relatively dense and highly oriented, while the interior appeared less compact, suggesting the presence of skin-core heterogeneity based on crack-propagation experiment results.[9,14] Li *et al.* observed brittle-fractured Kevlar 29 fibers using SEM and identified pronounced differences between the skin and core regions along the fracture plane.[15] These results obtained from the study of the skin-core structure come from the direct observation of the fiber morphology, and the skin thickness obtained depends very much on the experimental techniques used. Further work is necessary to understand this skin-core structure both quantitatively and at the molecular level.[16]

Experimental studies have shown that for PPTA fibers, both the elastic modulus and elongation at break, two essential mechanical properties, are dependent on crystallinity.[17] Therefore, crystallinity control during fiber preparation and processing plays an important role in determining fiber performance in advanced applications.[18] Roenbeck *et al.* exposed the internal cross-sections of several types of Kevlar fibers by focused ion beam (FIB) notching and observed by atomic force microscopy (AFM) mapping that the transverse stiffness of the cortex region was lower than that of the core; they attributed this contrast to a non-uniform crystallinity distribution.[19,20] Chabi *et al.* revealed the skin-core structure of

* Corresponding author, E-mail: zhsu@ciac.ac.cn
Received March 13, 2026; Accepted July 20, 2026; Published online September 10, 2026

Kevlar 29 fiber by SEM, assessed the local mechanical properties of the fiber using nanoindentation, and reported higher stiffness in the core than in the skin, thereby inferring lower crystallinity in the skin region.[20] In contrast, Li *et al.* analyzed the effects of solution dispersion and coagulation bath on the fiber formation process and concluded that the skin layer possesses a higher degree of crystallinity than the core.[21] Recently, Liu *et al.* performed synchrotron wide-angle X-ray scattering (WAXS) line-scanning on Kevlar 29 and reported that the crystallinity of the skin layer was lower than that of the core.[22]

Confocal Raman spectroscopy is a nondestructive optical technique with several key advantages, including rapid data acquisition, minimal sample preparation, and high spatial resolution. These features make it particularly well suited for probing the crystallinity of single fibers and localized microregions. For example, Laramee *et al.* studied electrospun poly(ethylene terephthalate) (PET) nanofibers using polarized confocal Raman spectroscopy and determined the molecular orientation and degree of crystallinity within the fibers collected, which helped clarify the effect of the collector on the internal structure of the electrospun fibers.[23] Sharma *et al.* visualized the crystallinity distribution by Raman mapping across the cross-section of PET monofilaments and PET-polyamide 6 (PA6) composite fibers, revealing a pronounced skin-core structure.[24] Recently, Sun *et al.* demonstrated analyses of degree of crystallinity[18] and molecular orientation[25] in individual PPTA fibers by confocal Raman spectroscopy with excellent agreement with that measured by WAXD. These studies indicate that confocal Raman spectroscopy can not only assess polymer crystallinity with accuracy, but also resolve spatially heterogeneous structures within fibers.

In this study, the skin-core structures of Kevlar 29 and Kevlar 49 fibers were investigated using confocal Raman spectroscopy. The results showed that the crystalline fraction in the core was higher than that in the skin in both cases, with a distinct radial crystallinity distribution.

EXPERIMENTAL

Materials

The two PPTA specimens examined were commercially available Kevlar 29 and Kevlar 49 fibers produced by DuPont, which were used as received without further treatment.

Sample Preparation

Individual fibers carefully straightened and aligned roughly parallel to each other were embedded in epoxy resin (SPI-Pon 812) and cut along the axial direction at room temperature using a diamond knife (DiATOME cryo 35°) on an ultramicrotome (RMC Boeckeler PT-PC). Thin sections of approximately 500–1000 nm thickness were collected and transferred onto a polished silicon wafer substrate for subsequent analyses.

Characterization

Spectra were acquired using a LabRAM HR 800 spectrometer (HORIBA) coupled with an Olympus BX 41 optical microscope in backscattering geometry with an excitation wavelength of 633 nm from a He-Ne laser operating at a power of 1.8 mW. The laser beam was focused onto the sample surface using a 100× objective lens with a numerical aperture of 0.9. Both confocal pinhole and slit widths were set to 20 μm. Raman signals were dispersed using a 600 g/mm grating and were recorded using a CCD camera. No discernible photothermal effects or irreversible spectral changes were observed during these measurements. The spectra were processed using OMNIC 8.2 software. To eliminate background contributions arising from fluorescence, polynomial baseline correction was applied to all spectra.

RESULTS AND DISCUSSION

Fig. 1 shows the Raman spectra of both the Kevlar 29 and Kevlar 49 fibers in the range of 600–1800 cm^{-1}. The two spectra are almost identical, exhibiting the characteristic bands of PPTA. Specifically, the band at 1280 cm^{-1} is assigned to coupled N—H bending, C—N stretching, and C—C stretching vibrations; the peak at 1332 cm^{-1} originates from ring C—H bending combined with aromatic C—C stretching; and the most prominent band at 1610 cm^{-1} corresponds to aromatic ring C—C stretching vibration.[26] In addition, the medium-intensity C=O stretching vibration (amide I band) appears at approximately 1650 cm^{-1}, which is highly sensitive to crystallinity and is regarded as one of the most important structural markers for distinguishing the crystalline and amorphous phases in PPTA fibers.[27,28] Previous studies have established that PPTA crystallization is promoted only when the C=O groups in the polymer chain adopt a trans conformation and are coplanar with the adjacent benzene rings, thereby enabling efficient chain packing.[29–31] Based on this structural model, Sun *et al.* deconvoluted the amide I band into multiple components for different conformations and developed a Raman-based quantitative method for determining the crystallinity of individual PPTA fibers.[18] This method also allows the assessment of local crystallinity variations within a single fiber.

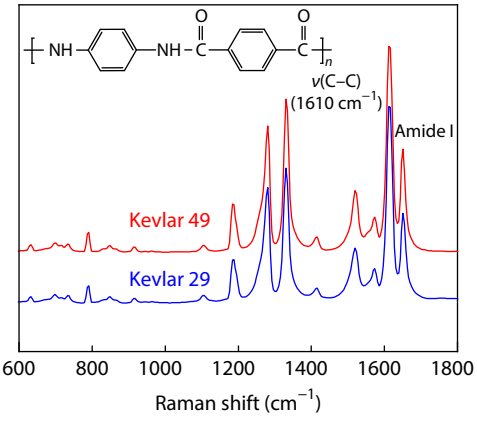

Fig. 1 Raman spectra of Kevlar 29 and Kevlar 49 fibers in the 600–1800 cm^{-1} region.

Because of the strong scattering and absorption of the excitation light by the PPTA fiber, direct analysis of the core region by focusing the laser inside the fiber produced poor-quality Raman spectra with low signal intensities. Therefore, the fibers were embedded in epoxy resin and cut along the axial direction *via* ultramicrotomy to produce longitudinal cross-sections of the fibers.[16] We employed longitudinal cross-sections instead of lateral ones so that the Raman ex-

https://doi.org/10.1007/s10118-026-3822-3

perimental geometry was consistent with that in the crystallinity quantitation method established,[18] as illustrated in Fig. S2 (in the electronic supplementary information, ESI). This is important because the excitation laser is polarized and the PPTA chains are not randomly oriented. As a result, the Raman spectra acquired from the longitudinal cross-section match well with those from the fiber, whereas the spectra from the lateral cross-section are different and the quantitation method established in Ref. [18] is not applicable. From the optical images shown in Fig. 2, longitudinal sections of the Kevlar fibers are clearly observed, the width of which is approximately 13–15 μm, which corresponds to the diameter of the fibers, and the boundary between the epoxy resin and the aramid fiber is clearly distinguishable. This well-defined morphology facilitates reliable Raman spectral acquisition from both the skin and core regions of the fiber.

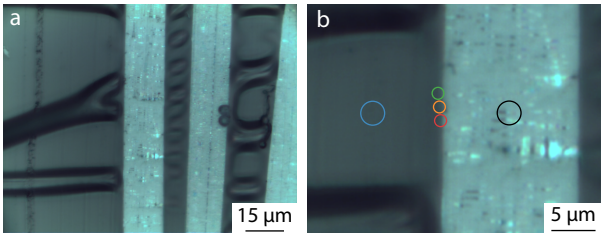

Fig. 2 (a, b) Optical microscopy images of longitudinal sections of Kevlar fibers embedded in epoxy resin. The color circles in (b) mark the positions where spectra in Fig. 3 are acquired.

Previous studies have revealed that the thickness of the skin layer of Kevlar fibers is typically in the range of 0.1–1 μm.[31] The lateral spatial resolution of confocal Raman spectroscopy can be estimated based on the Rayleigh diffraction limit as $d_{XY} \approx 0.61\lambda/NA$, where λ is the excitation wavelength and *NA* is the numerical aperture of the objective lens.[32] Thus, the lateral spatial resolution achieved using the 100× objective (*NA ca.* 0.9) and 633 nm excitation laser was on the order of about 1 μm. In practical measurements, instrumental adjustments made to achieve an acceptable spectral quality, such as confocal pinhole size, focus conditions, and signal-to-noise optimization, can significantly influence the actual probing volume. Consequently, the effective lateral resolution in the measurements was approximately 2 μm, which is significantly larger than the reported skin-layer thickness. Owing to this instrumental limitation, we were not able to directly target the skin layer for spectral acquisition. Instead, Raman spectra were acquired stepwise from the surrounding epoxy resin region toward the fiber region (Fig. 2b). By analyzing the intensity evolution of the Raman bands characteristic of PPTA in comparison with that of the resin, the proximity of the measurement position to the fiber skin layer could be inferred. As shown in Fig. 3(a), the spectrum (blue trace) collected in the matrix region far from the fiber matches that of the epoxy, dominated by a strong band at *ca.* 1450 cm^{-1} assigned to the methylene bending vibration, and the carbonyl stretching of the ester groups at *ca.* 1700–1780 cm^{-1}.[33,34] No PPTA features are observed. As the laser focal spot gradually approaches the fiber, peaks characteristic of PPTA, in particular the aromatic ring C—C stretching bands at 1610 and 1518 cm^{-1}, begin to emerge in the resin-dominated spectra, indicating the contribution from the skin region of the fiber. The PPTA features become progressively more intense, and when the laser focal spot moves within the fiber (black trace), the epoxy characteristics at 1450 and 1740 cm^{-1} completely disappear, and the spectrum matches that of PPTA shown in Fig. 1. The spectra for the skin layer were then obtained by subtracting the epoxy contribution from the spectra recorded at the perimeter of the fiber (Fig. 3b). The resin-specific band at 1740 cm^{-1} was selected as the reference peak for subtraction, as no PPTA-related Raman band was present in this region. The subtraction process was considered complete when the intensity of the 1740 cm^{-1} band was reduced to zero, yielding a resin-free Raman spectrum for the skin layer. Consistent results were obtained using a different subtraction protocol (Fig. S3 and Table S1 in ESI), thereby indicating the validity and robustness of the proposed method. The amide I band is not distorted during this process (Fig. S4 and Table S2 in ESI) and is suitable for subsequent crystallinity analysis.

The crystallinity-sensitive amide-I regions of the spectra obtained for the skin and core regions of Kevlar 29 are compared in Fig. 4(a). A subtle shift in the position of the band at approximately 1650 cm^{-1} is observed for the skin region toward higher wavenumbers relative to that of the core region. This shift is more discernible in Fig. S5 (in ESI), which shows multiple spectra collected from different skin and core regions. It has been reported that the amide I bands for the

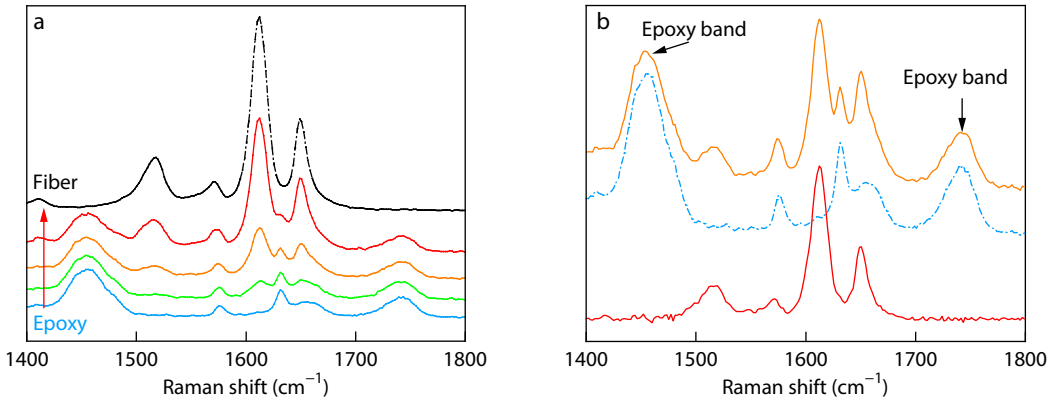

Fig. 3 (a) Raman spectra acquired at different positions marked by colored circles in Fig. 2(b). (b) Subtraction of the epoxy contribution (blue) from the mixed spectrum (orange) yields the spectrum for the skin layer (red).

https://doi.org/10.1007/s10118-026-3822-3

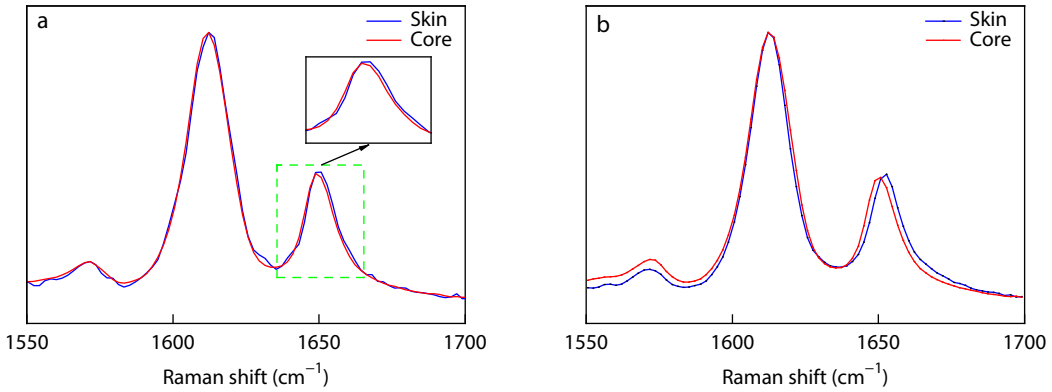

Fig. 4 Comparison of Raman spectra between skin (blue) and core (red) regions of (a) Kevlar 29 and (b) Kevlar 49 fibers.

amorphous and crystalline phases are located at 1652 and 1648 cm^{-1}, respectively,[18,27] so this peak shift to higher wavenumbers suggests lower crystallinity[35] in the skin region. To verify this finding, the degrees of crystallinity in both the skin and core of Kevlar 29 were extracted from their Raman spectra using the method developed by Sun *et al.*[18] Briefly, the amide I band at about 1650 cm^{-1} was deconvoluted into three sub-bands located at approximately 1633, 1649, and 1662 cm^{-1}, assigned to *cis*, in-plane *trans* and out-of-plane *trans* conformations, respectively (Fig. 5), and the crystallinity was derived using the following equation:[18]

$$X = (I_{1649} - I_{1662})/(I_{1633} + I_{1649} + I_{1662}) \quad (1)$$

where X is the degree of crystallinity, and I is the intensity (area) of the sub-band.

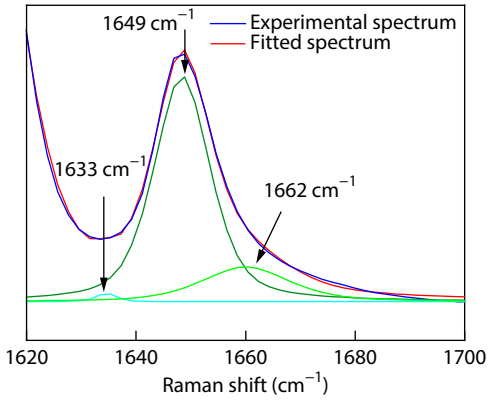

Fig. 5 Schematic illustration of the deconvolution of the amide I band into three components.

To increase the reliability of the experiment, three distinct positions were selected from one fiber for both the skin and core regions, and three spectra were collected at each position, producing nine replicate spectra for each region. The average degree of crystallinity determined for the center region (the bulk part of the fiber) was 62.1%±1.7%, which is in good agreement with the literature value for Kevlar 29 fibers.[22] In contrast, the crystallinity in the skin region was 54.4%±2.5%, which was significantly lower than that in the core. Thus, both the qualitative observation based on the amide I band position and the quantitative analysis result demonstrate that the crystallinity at the fiber center is higher than that at the edge, providing clear evidence for the skin-core heterogeneity in aramid fibers.[22]

To further elucidate the crystallinity distribution in the radial direction, a line-scan analysis was performed, where Raman spectra were acquired along the radial direction from the perimeter region toward the fiber center at a step size of 200–500 nm, and the spectra were then processed as described above. It should be emphasized again that the spatial resolution was 2 μm, indicating a significant overlap in the sampling volume between neighboring points. The line-scan measurements were performed at three different locations on the same fiber, and the averages are reported. Fig. 6(a) shows the degree of crystallinity derived from the Raman spectra as a function of the radial position for Kevlar 29. We see that the crystallinity at the fiber surface is rather low at *ca.* 50%, which rises quickly to just below 60% in the first several steps, and then continues to increase slowly to *ca.* 63% at the fiber center.

The Raman analysis results clearly revealed a heterogeneous distribution in crystallinity along the radial direction in the Kevlar 29 fiber, with the skin region significantly less crystalline than the core, exhibiting a pronounced gradient. This distinct morphological feature can be rationally interpreted based on the formation mechanism of the aramid fibers reported previously.[14] During the fiber spinning process, PPTA chains in the skin region experience higher shear stress and hence attain a higher degree of orientation than that in the core,[16,36] however, in the subsequent coagulation stage, the skin region undergoes rapid cooling, effectively "freezing" the highly oriented molecular structure formed during spinning.[9,36] As a result, the chain ends are randomly distributed, disrupting the formation of extended-chain crystals of PPTA.[9] In contrast, the core region retains a longer relaxation time, allowing more extensive molecular chain rearrangement and solvent-coagulant exchange; thus, the ionic chain ends, driven by both electrostatic interactions and steric factors, can aggregate within planes perpendicular to the fiber axis, leading to a higher degree of crystallinity.[9,36]

The same analysis was applied to the Kevlar 49 fiber. Fig. 4(b) displays the amide I region of the Raman spectra for the skin and core of the fiber, which shows a more pronounced peak position shift between the two than that for Kevlar 29, implying a greater crystallinity difference between the surface and the interior in Kevlar 49. This is confirmed by the radial crystallinity distribution profile shown in Fig. 6(b). Com-

https://doi.org/10.1007/s10118-026-3822-3

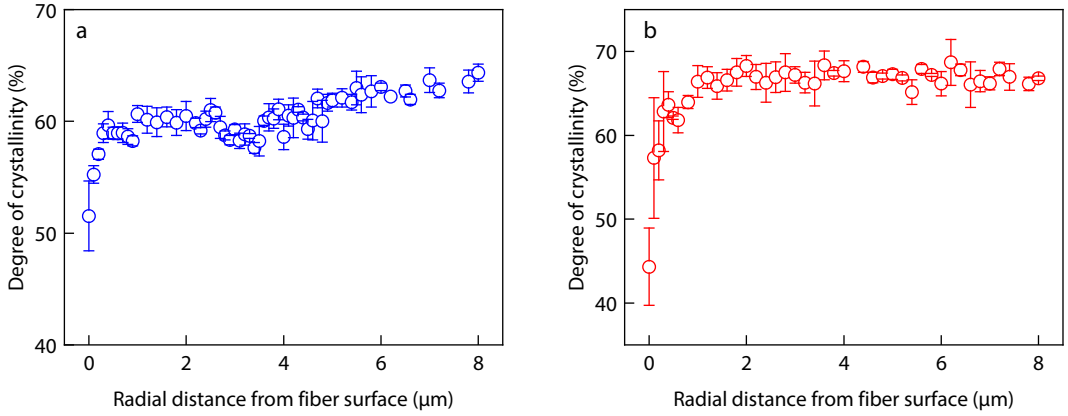

Fig. 6 Radial crystallinity distribution of PPTA fiber cross-section for (a) Kevlar 29, and (b) Kevlar 49.

pared with Kevlar 29, the transition from the low-crystallinity region to the high-crystallinity region was steeper, suggesting a thinner skin layer in Kevlar 49 and a substantially greater proportion of the core than in Kevlar 29, consistent with that observed by Roenbeck.[19,20] In addition, the core region of Kevlar 49 exhibited a higher crystallinity of *ca.* 68% and a more uniform crystallinity distribution than Kevlar 29. The difference in crystallinity and radial distribution observed between the two fibers is likely due to their distinct processing and post-treatment histories. It has been reported that Kevlar 49 is obtained from Kevlar 29 through subsequent stretching and thermal treatment,[37] and such treatment can reduce microvoids and structural heterogeneities, thereby promoting structural homogenization and enhancing overall crystallinity,[37] resulting in a higher elastic modulus for Kevlar 49 than for Kevlar 29. The higher and more uniform crystallinity observed in Kevlar 49 in the present study is consistent with previous findings.[37]

CONCLUSIONS

In this study, confocal Raman spectroscopy was employed to quantitatively analyze the skin-core crystallinity heterogeneity in PPTA fibers, using Kevlar 29 and Kevlar 49 as examples. The results clearly show that the crystallinity of the fiber core was significantly higher than that of the skin region for both fibers. Profile analysis of the radial crystallinity distribution revealed a continuous gradient from the skin to the core, rather than a sharp skin-core interface. Kevlar 49 showed a steeper transition from the skin to the core and a more uniform distribution of crystallinity in the core region than Kevlar 29, exhibiting a higher degree of crystallinity. These findings provide structural insights for a better understanding of the structure-property relationship of aramid fibers.

Conflict of Interests

The authors declare no interest conflict.

Electronic Supplementary Information

Electronic supplementary information (ESI) is available free of charge in the online version of this article at http://doi.org/10.1007/s10118-026-3822-3.

Data Availability Statement

The data are available from the corresponding author upon reasonable request.

ACKNOWLEDGMENTS

This work was financially supported by the Department of Science and Technology of Jilin Province (No. SKL202402012).

REFERENCES

1 Machalaba, N. N.; Perepelkin, K. E. Heterocyclic aramide fibers–production principles, properties and application. *J. Ind. Text.* **2002**, *31*, 189–204.
2 Tikhonov, I. V.; Tokarev, A. V.; Shorin, S. V.; Shchetinin, V. M.; Chernykh, T. E.; Bova, V. G. Russian aramid fibres: past – present – future. *Fibre Chem.* **2013**, *45*, 1–8.
3 Zhang, W.; Wang, Y.; Sun, G.; Wang, C.; Li, C.; Xiao, C. Super fine para-aramid nanofiber and membrane fabricated by airflow-assisted coaxial spinning. *Polymer* **2024**, *311*, 127566.
4 Keten, S.; Xu, Z.; Ihle, B.; Buehler, M. J. Nanoconfinement controls stiffness, strength and mechanical toughness of β-sheet crystals in silk. *Nat. Mater.* **2010**, *9*, 359–367.
5 Launey, M. E.; Ritchie, R. O. On the fracture toughness of advanced materials. *Adv. Mater.* **2009**, *21*, 2103–2110.
6 Jia, Y.; Wang, H.-L.; Liu, B.; Huang, Y.; Gao, H. Intrinsic-to-extrinsic transition in fracture toughness through structural design: a lesson from nature. *Extreme Mech. Lett.* **2020**, *37*, 100685.
7 Ritchie, R. O. Toughening materials: enhancing resistance to fracture. *Phil. Trans. R. Soc. A* **2021**, *379*, 20200437.
8 Akato, K.; Bhat, G. *Structure and Properties of High-Performance Fibers*, 1st ed.; Woodhead Publishing: Cambridge, UK, **2017**, pp. 245–266.
9 Morgan, R. J.; Pruneda, C. O.; Steele, W. J. The relationship between the physical structure and the microscopic deformation and failure processes of poly(p-phenylene terephthalamide) fibers. *J. Polym. Sci. Polym. Phys. Ed.* **1983**, *21*, 1757–1783.
10 Riekel, C.; Cedola, A.; Heidelbach, F.; Wagner, K. Microdiffraction experiments on single polymeric fibers by synchrotron radiation. *Macromolecules* **1997**, *30*, 1033–1037.
11 Roth, S.; Burghammer, M.; Janotta, A.; Riekel, C. Rotational

Graphical Abstract

Radial Distribution of Crystallinity in Aramid Fibers Investigated by Raman Spectroscopy

Wei-Gen Yang, Yuan Lin, Hao-Jun Sun, and Zhao-Hui Su

Changchun Institute of Applied Chemistry, Chinese Academy of Sciences; University of Science and Technology of China

Quantitative analysis using confocal Raman spectroscopy revealed skin-core heterogeneity in the Kevlar fibers, where the crystallinity in the core region was significantly higher than that in the skin.

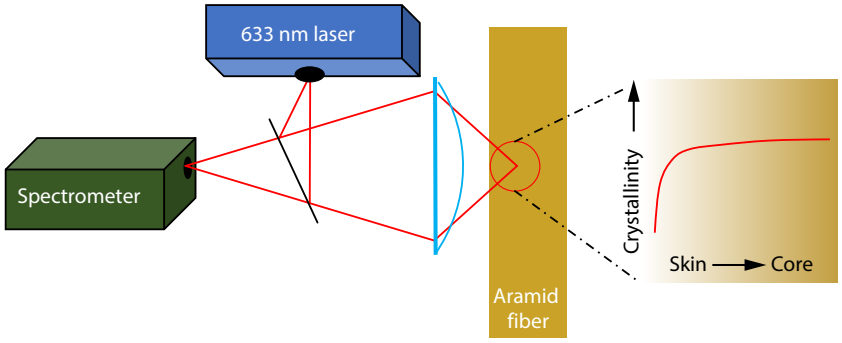

Chinese J. Polym. Sci. 2026 *https://doi.org/10.1007/s10118-026-3822-3*

disorder in poly(p-phenylene terephthalamide) fibers by X-ray diffraction with a 100 nm beam. *Macromolecules* **2003**, *36*, 1585–1593.

12 Kitagawa, T. Novel fine structures in poly-p-phenylenebenzobisoxazole fibers induced by water vapor, hot water, and non-aqueous coagulation I molecular orientation along the fiber axis and fine structures. *J. Macromol. Sci. Part B* **2015**, *54*, 1323–1340.

13 Dobb, M. G.; Johnson, D. J.; Saville, B. P. Supramolecular structure of a high-modulus polyaromatic fiber (Kevlar 49). *J. Polym. Sci. Polym. Phys. Ed.* **1977**, *15*, 2201–2211.

14 Morgan, R. J.; Pruneda, C. O. The characterization of the chemical impurities in Kevlar 49 fibres. *Polymer* **1987**, *28*, 340–346.

15 Li, L. S.; Allard, L. F.; Bigelow, W. C. On the morphology of aromatic polyamide fibers (Kevlar, Kevlar-49, and PRD-49). *J. Macromol. Sci. Part B* **1983**, *22*, 269–290.

16 Young, R. J.; Lu, D.; Day, R. J.; Knoff, W. F.; Davis, H. A. Relationship between structure and mechanical properties for aramid fibres. *J. Mater. Sci.* **1992**, *27*, 5431–5440.

17 Hindeleh, A. M.; Halim, N. A.; Ziq, K. A. Solid-state morphology and mechanical properties of Kevlar 29 fiber. *J. Macromol. Sci. Part B* **1984**, *23*, 289–309.

18 Sun, H.; Meng, X.; Luo, C.; Qian, Y.; Men, Y.; Su, Z. Quantifying crystallinity in poly(*p*-phenylene terephthalamide) by Raman spectroscopy. *Macromolecules* **2024**, *57*, 7390–7397.

19 Roenbeck, M. R.; Sandoz-Rosado, E. J.; Cline, J.; Wu, V.; Moy, P.; Afshari, M.; Reichert, D.; Lustig, S. R.; Strawhecker, K. E. Probing the internal structures of Kevlar® fibers and their impacts on mechanical performance. *Polymer* **2017**, *128*, 200–210.

20 Roenbeck, M. R.; Cline, J.; Wu, V.; Afshari, M.; Kellner, S.; Martin, P.; Londono, J. D.; Clinger, L. E.; Reichert, D.; Lustig, S. R.; Strawhecker, K. E. Structure–property relationships of aramid fibers *via* X-ray scattering and atomic force microscopy. *J. Mater. Sci.* **2019**, *54*, 6668–6683.

21 Li, Y.; Hu, Z.; Ma, Y.; Yu, J.; Zhu, J.; Wang, Y. The influences of coagulation bath conditions on para-aramid formation. *Hi-Tech Fiber and Application* **2015**, *40*, 24–27.

22 Liu, P.; Zhang, Z.; Zhu, H.; Deng, X.; Li, Z.; Li, Y.; Lv, J.; Zhang, D.; Liu, X.; Luo, L. Skin-core structural homogeneity and stress-induced ordering enable extrinsic toughening in rigid-chain heterocyclic aramid fibers. *Macromolecules* **2025**, *58*, 9358–9372.

23 Laramée, A. W.; Lanthier, C.; Pellerin, C. Raman investigation of the processing structure relations in individual poly (ethylene terephthalate) electrospun fibers. *Appl. Spectrosc.* **2022**, *76*, 51–60.

24 Sharma, K.; Braun, O.; Tritsch, S.; Muff, R.; Hufenus, R.; Perret, E. 2D Raman, ATR-FTIR, WAXD, SAXS and DSC data of PET mono- and PET/PA6 bicomponent filaments. *Data Brief* **2021**, *38*, 107416.

25 Sun, H.; Jia, T.; Qian, Y.; Chen, Q.; Men, Y.; Su, Z. Quantifying molecular orientation in poly(p-phenylene terephthalamide) fibers by polarized Raman spectroscopy. *Polymer* **2025**, *325*, 128310.

26 Kim, P. K.; Chang, C.; Hsu, S. L. Normal vibrational analysis of a rigid rod polymer: poly(p-phenylene terephthalamide). *Polymer* **1986**, *27*, 34–46.

27 Gonzalez, G. M.; MacQueen, L. A.; Lind, J. U.; Fitzgibbons, S. A.; Chantre, C. O.; Huggler, I.; Golecki, H. M.; Goss, J. A.; Parker, K. K. Production of synthetic, para-aramid and biopolymer nanofibers by immersion rotary jet-spinning. *Macromol. Mater. Eng.* **2017**, *302*, 1600365.

28 Bouita, M.; Tinnes, J.-P.; Bourson, P.; Malfois, M.; Ponçot, M. A new Raman spectroscopy-based method for monitoring the crystallinity ratio of polyethylene terephthalate. *J. Raman Spectrosc.* **2023**, *54*, 225–232.

29 Bouita, M.; Tinnes, J. P.; Ponçot, M. Monitoring the thermal behavior of polyethylene 2,5-furandicarboxylate using Raman spectroscopy. *J. Raman Spectrosc.* **2023**, *54*, 683–690.

30 Lebeau, C.; Guillou, H.; Tessier, C.; Brisson, J. Electron diffraction

and molecular modelling investigation of the crystal structure of poly(para-phenylene terephthalamide) form II. *Polymer* **2011**, *52*, 4083–4092.
31 Dobb, M. G.; Robson, R. M. Structural characteristics of aramid fibre variants. *J. Mater. Sci.* **1990**, *25*, 459–464.
32 El-Mashtoly, S. F., *Confocal Raman Microscopy*, 2nd ed.; Springer: Cham, Switzerland, **2019**, pp. 72–87.
33 Chike, K. E.; Myrick, M. L.; Lyon, R. E.; Angel, S. M. Raman and near-infrared studies of an epoxy resin. *Appl. Spectrosc.* **1993**, *47*, 1631–1635.
34 Morsch, S.; Liu, Y.; Lyon, S. B.; Gibbon, S. R.; Gabriele, B.; Malanin, M.; Eichhorn, K. J. Examining the early stages of thermal oxidative degradation in epoxy-amine resins. *Polym. Degrad. Stab.* **2020**, *176*, 109147.
35 Gonzalez, G. M.; Ward, J.; Song, J.; Swana, K.; Fossey, S. A.; Palmer, J. L.; Zhang, F. W.; Lucian, V. M.; Cera, L.; Zimmerman, J. F.; Burpo, F. J.; Parker, K. K. Para-aramid fiber sheets for simultaneous mechanical and thermal protection in extreme environments. *Matter* **2020**, *3*, 742–758.
36 Takahashi, T.; Iwamoto, H.; Inoue, K.; Tsujimoto, I. Quiescent and strain-induced crystallization of poly(*p*-phenylene terephthalamide) from sulfuric acid solution. *J. Polym. Sci. Polym. Phys. Ed.* **1979**, *17*, 115–122.
37 Wang, R. M.; Zheng, S. R.; Zheng, Y. P. Reinforced materials. In *Polymer Matrix Composites and Technology*, 1st ed.; Woodhead Publishing: Cambridge, UK, **2011**, pp. 29–548.

https://doi.org/10.1007/s10118-026-3822-3